Modelling Techniques

Representation of atmospheric blocking in the new global non-hydrostatic weather prediction model ICON

Roman Attinger[1*], Julia H. Keller[2], Martin Köhler[2], Jacopo Riboldi[1,3] and Christian M. Grams[1,4]

[1]Institute for Atmospheric and Climate Science, ETH Zurich, Switzerland
[2]Deutscher Wetterdienst, Offenbach, Germany
[3]Current affiliation: Laboratoire de Météorologie Dynamique/IPSL, École Normale Supérieure, PSL Research University, CNRS, Paris, France
[4]Current affiliation: Institute for Meteorology and Climate Research (IMK-TRO), Karlsruhe Institute of Technology (KIT), Karlsruhe, Germany

Abstract

The correct depiction of atmospheric blocking still poses a key challenge for current numerical weather prediction (NWP) and climate models. This study evaluates the representation of blocking in the new global ICOsahedral Non-hydrostatic NWP and climate model ICON and links model mean state biases to observed blocking deviations. Blocking is identified using both an anomaly and a flow reversal approach in an eight member ensemble of 15-year AMIP-type ICON simulations and verified against ERA Interim reanalyses. Either approach demonstrates a good representation of annual blocking frequencies in ICON. Deviations emerge when considering individual seasons. In the anomaly framework, enhanced blocking occurrence in the mid-latitude Pacific domain during winter and spring and a marked underestimation of blocking in the Euro-Atlantic region are found during summer. Moreover, this approach indicates a general underestimation of blocking at higher latitudes. The flow reversal index reveals the often reported underestimation of blocking in the Euro-Atlantic region during winter. Furthermore, increased blocking activity in the Pacific and Greenland region during spring and decreased blocking occurrence at high latitudes in summer are found. Focusing on the anomaly approach, we assess how the model mean state influences blocking identification. A systematically higher tropopause, forced by a cold bias in the lower stratosphere, reduces diagnosed blocking frequencies at higher latitudes especially during summer. This goes along with a reduction in blocking size, duration, and intensity. While confirming an overall good representation of blocking in ICON, this study demonstrates how mean state biases can crucially affect the identification of blocking and that blocking deviations have to be interpreted with caution as they are highly dependent on the exact diagnostic used.

Keywords: atmospheric blocking, ICON, blocking identification, model evaluation, Northern Hemisphere

1 Introduction

Atmospheric blocking is a key driver of large-scale flow variability in the mid-latitudes, and as such an integral part of medium-range predictability (e.g. Matsueda and Palmer, 2018). Blocking is defined as a persistent, quasi-stationary high-pressure system which disrupts the mean upper-level westerly flow and is generally observed at the end of the Atlantic and Pacific storm track (Rex, 1950). Due to its persistence and deep structure, blocking is able to deflect transient eddies north- and southward, leading to the modulation of temperature and precipitation patterns in the blocked and adjacent region (e.g. Buehler et al., 2011). High-impact weather conditions, such as heat waves (e.g. Black et al., 2004; Quandt et al., 2019), cold spells (e.g. Pfahl and Wernli, 2012; Bieli et al., 2015) or extreme precipitation events (e.g. Martius et al., 2013;

Grams et al., 2014; Piaget et al., 2015; Lenggenhager et al., 2018; Pasquier et al., 2019) can be associated with blocking.

Various methods to objectively define blocking in both observational and numerical weather prediction (NWP) model data exist. Following the early work by Rex (1950), who subjectively defined blocking based on the sharp transition of westerly to meridional flow, numerous indices have been developed that identify blocking as the reversal of an absolute field (e.g. Tibaldi and Molteni, 1990; Pelly and Hoskins, 2003; Scherrer et al., 2006; Davini et al., 2012). Conversely, anomaly based approaches focus on the anticyclonic anomaly inherent to blocking (e.g. Elliott and Smith, 1949; Dole and Gordon, 1983; Schwierz et al., 2004; Small et al., 2013). Depending on the exact definition used, differing blocking patterns and frequencies emerge. Barriopedro et al. (2010) provide an in-depth review of the performance of current blocking indices.

*Corresponding author: Roman Attinger, ETH Zurich, Universitätstrasse 16, 8092 Zurich, Switzerland, e-mail: roman.attinger@env.ethz.ch

Extensive research on the representation of blocking in general circulation models (GCMs) has revealed that its correct simulation is crucial for an accurate depiction of the large-scale flow variability in the mid-latitudes. While results are strongly dependent on the blocking diagnostic used, GCMs generally tend to underestimate the climatological occurrence of blocking, especially over Europe (e.g. DOBLAS-REYES et al., 1998; MASATO et al., 2013; ANSTEY et al., 2013). It has been shown that increasing the horizontal resolution or implementing a stochastic physics scheme leads to a significant improvement of blocking depiction (e.g. MATSUEDA et al., 2009; BERCKMANS et al., 2013; DAWSON and PALMER, 2014; DAVINI and D'ANDREA, 2016). However, in some models, increasing the resolution only improves blocking representation in the Euro-Atlantic region, while Pacific blocks are unaffected (SCHIEMANN et al., 2017). Mean state biases, e.g. of the sea-surface temperature (SST) or jet strength, can further deteriorate the simulation of blocking (e.g. D'ANDREA et al., 1998; SCAIFE et al., 2010; VIAL and OSBORN, 2011). Furthermore, CROCI-MASPOLI and DAVIES (2009) and recently PFAHL et al. (2015) highlighted the importance of diabatic processes in the blocking life cycle, which might explain the poor skill in simulating blocking at low resolution. In the light of climate change and the growing demand for sub-seasonal as well as seasonal forecasts of improved accuracy, assessing the representation of atmospheric blocking in current GCMs is therefore crucial.

The ICOsahedral Non-hydrostatic NWP model ICON is a joint development of the Max-Planck-Institute for Meteorology (MPI-M) and the German Meteorological Service (DWD). ICON features fully compressible equations of motion, local mass conservation, and is based on an icosahedral-triangular grid (ZÄNGL et al., 2015). Such a grid has the advantage of avoiding singularities over the pole and reducing the area variance per grid cell. The dynamical core and ICON as a whole are designed in a seamless approach for applications ranging from limited area large-eddy simulations, via daily global NWP, to multi-year climate simulations. ICON is operational as NWP system at DWD since January 2015, producing 7-day forecasts at a global horizontal resolution of 13 km and 6.5 km over Europe.

The objective of the present study is to document the representation of blocking in the Northern Hemisphere in a recent operational NWP version of ICON. Blocking occurrence is computed using an anomaly based and flow reversal approach and compared to reanalyses. Moreover, we assess model mean state biases and investigate how they influence blocking identification in the anomaly framework. The paper is outlined as follows. The model specification, data, and blocking diagnostics are introduced in Section 2. A detailed assessment of the geographical blocking distribution and blocking characteristics in ICON is presented in Section 3. Model mean state biases, together with possible explanations for observed blocking frequency deviations, are discussed in

Section 4. Finally, we summarize our main findings and discuss implications thereof for future work in Section 5.

2 Data and methods

2.1 Data

An eight member ensemble of 15-year ICON simulations forms the data basis of this study. The lower boundary conditions are forced by monthly mean sea ice and sea surface temperatures from ERA-Interim for the period 2001 to 2015, which are linearly interpolated to yield slowly varying daily fields (following the established AMIP procedure according to GATES, 1992). To mimic initial condition perturbations, individual members are initialized using a time-lagged, irregularly spaced series of starting dates ranging from 0000 UTC on 1 August 2000 to 1800 UTC on 8 August 2000. The model uses an approximate icosahedral horizontal grid resolution of 80 km with 90 vertical levels from the surface up to 75 km. The data is interpolated to a regular grid at 1° horizontal resolution, 19 pressure levels reaching from 1000 hPa to 1 hPa and is available at 6-hourly temporal resolution.

European Centre for Medium-Range Weather Forecasts Re-Analysis Interim (ERA-Interim) data (DEE et al., 2011) for the period 1979 to 2016 are used as reference and considered as being representative of the actual state of the atmosphere. ERA-Interim data are available at 6-hourly temporal and 1°×1° spatial resolution and on the same 19 pressure levels as ICON.

Because specific humidity is not constrained in reanalyses (e.g. FUJIWARA et al., 2017; DAVIS et al., 2017), water vapour measurements from the Microwave Limb Sounder (MLS) satellite (WATERS et al., 2006) for the period 1991 to 2012 are used to assess the representation of specific humidity in ICON.

2.2 Blocking identification

Blocking is identified using the potential vorticity (PV) based anomaly index (APV*) introduced by SCHWIERZ et al. (2004). This approach exploits the fact that atmospheric blocking can be diagnosed as a region of anomalously low-PV below the dynamical tropopause. To this end, Ertel PV (ERTEL, 1942) is computed on pressure levels and vertically averaged from mid-tropospheric (500 hPa) to lower-stratospheric (150 hPa) levels. Vertically averaged PV (VAPV) anomalies are computed by subtracting the monthly VAPV climatology pertaining to each of the ICON ensemble members and ERA-Interim, respectively, from the instantaneous VAPV fields. In order to filter out the high frequency fluctuations associated with transient eddies, the resulting VAPV anomalies are subject to a two-day running mean before blocking is computed. Consistent with earlier studies (e.g. CROCI-MASPOLI et al., 2007; PFAHL et al., 2015), an instantaneously blocked region is then

identified as a closed contour of VAPV anomaly exceeding ≤ −1.3 PVU and satisfying a spatial overlap of 70 % between two subsequent 6-hourly time steps for at least 5 consecutive days. Blocking frequencies obtained using this approach are descriptive of the fraction of blocked time steps at any given grid point.

Other studies often adopt a reversal based blocking index for the assessment of blocking in GCMs instead of an anomaly based approach. To aid comparison of our results with these studies, we additionally apply the two-dimensional (2D) absolute geopotential height (AGP) index by SCHERRER et al. (2006), which is based on the mono-dimensional index introduced by TIBALDI and MOLTENI (1990). For blocking to be identified, this index requires a reversal of the longitudinal gradient on the 500 hPa geopotential height field to the south and westerly flow to the north during at least 5 consecutive days at any grid point between 35° and 75° N. Refer to SCHERRER et al. (2006) for a detailed discussion of both the APV* and AGP index.

2.3 Assessment of statistical significance

The 15-year AMIP-type simulations realized for this study allow the model to develop its own internal dynamics and equilibrium state which is not restricted by observations. To assess robust deviations of individual ICON ensemble members and the ensemble mean from reanalysis, a Monte Carlo re-sampling technique is applied to annual and seasonal blocking frequencies computed from ERA-Interim. To this end, 1000 random 15-year samples are selected from reanalysis and mean annual (and seasonal) blocking frequencies in each sample are computed. ICON blocking frequencies that exceed the 2.5 to 97.5 interquantile range of the resampled blocking frequency distribution are thereby defined as significantly deviating from reanalysis.

Beyond the blocking frequencies, we also assess the seasonal mean state of meteorological fields in ICON. Namely, we investigate the three-dimensional representation of potential temperature (TH), PV, specific humidity (Qv) and the zonal wind component (U). Seasonal means from ERA-Interim and MLS are subject to a random 1000 trial 15-year re-sampling to obtain a robust baseline for the evaluation of the ICON mean state.

3 Blocking representation

This section describes the simulation of blocking in ICON with respect to ERA-Interim as observed using the APV* index (Section 3.1), followed by the flow reversal approach (Section 3.2), and finally APV* blocking characteristics are discussed in Section 3.3.

3.1 APV* blocking climatology

The annual blocking frequency distribution as identified by the APV* index is shown in Fig. 1a. Colors describe the average blocking occurrence of the eight ICON ensemble members while the black contours depict the re-sampled ERA-Interim mean. The APV* approach identifies three regions of increased blocking activity; one each at the exit region of the Atlantic and Pacific storm track and one over northern Russia. This is consistent with other studies that use an anomaly based blocking identification (e.g. DOLE and GORDON, 1983; CROCI-MASPOLI et al., 2007; SMALL et al., 2013). According to reanalysis, blocking over the Atlantic is slightly more frequent than blocking over the Pacific (13 % vs. 11 %, respectively 47 and 40 blocked days). The shading in Fig. 1b describes significant (dark colors) and non-significant (light colors) APV* blocking deviations from ERA-Interim as defined in Section 2.3. Both the Atlantic and Pacific peaks are well captured in ICON, as only non-significant deviations occur. Significant deviations from reanalysis are mainly confined to areas of lower blocking occurrence in the mid-latitudes and in the region of the Russian blocking maxima. Two features stand out: A band of increased blocking frequencies at the end of the climatological Pacific jet stream as well as a broad region of blocking underestimation of about 2 % (7 days) over the Eurasian continent.

To assess the simulation of blocking in different regions, sectors centered on the location of maximum blocking activity in ERA-Interim are introduced. These are defined as (i) the Euro-Atlantic (EA) sector ranging from 65° W to 0° E and (ii) the Pacific (PAC) sector encompassing 168° E to 124° W (each from the equator to the pole, see red dashed lines in Fig. 1b).

Using these sectors, a quantitative assessment of the annual mean, zonally averaged blocking occurrence is carried out. Deviations of the ICON ensemble mean and individual ensemble members from ERA-Interim are presented in Fig. 2. The inter-annual variability inherent to a random 15-year period of the re-sampled ERA-Interim mean is indicated by the 2.5 to 97.5 percentile confidence interval (grey area). Zonal blocking frequencies in ICON are mostly within this range (blue lines). Significant deviations from reanalysis are confined to the mid-latitudes in all sectors, i.e. where the ICON mean (red line) exceeds the confidence interval from ERA-Interim. Towards higher latitudes, blocking tends to be reduced by about 1 % and a significant underestimation is found toward the pole in the EA sector. The increase in blocking activity in the PAC mid-latitude region is highly robust, as each ensemble member exceeds the 97.5 percentile of ERA-Interim. These findings confirm that the largest deviations from reanalysis are located in the mid-latitudes, as previously indicated by the 2D maps of annual blocking frequency deviations (Fig. 1b).

A more complete picture can be obtained when considering different seasons individually. First, we describe the seasonal variation of APV* blocking as observed in ERA-Interim (black contours in Fig. 3). Maximum blocking frequencies in the EA region peak at around 13.5 % and are largely independent of the sea-
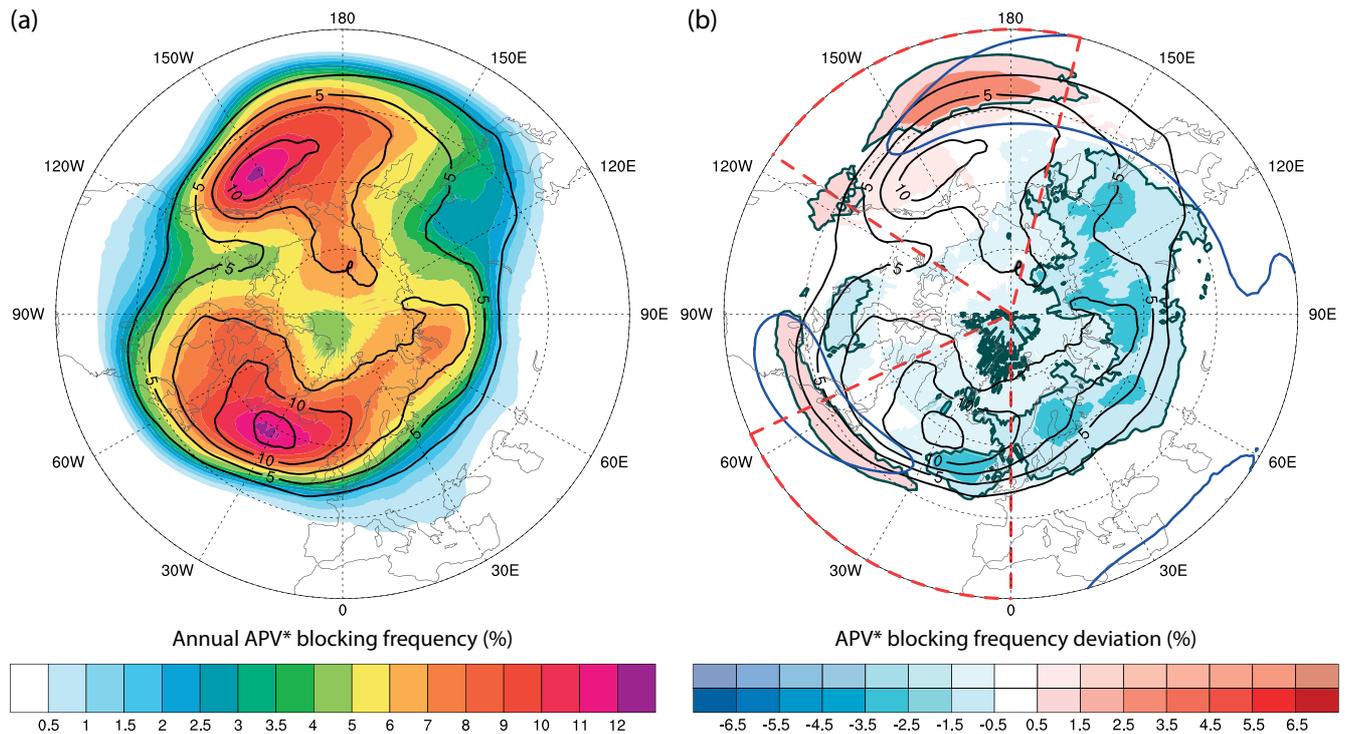
Figure 1: Annual APV* blocking distribution in ICON (a) and deviation from ERA-Interim (b). Blocking frequencies describe the number of blocked days per year, i.e. 9 % corresponds to about one fully blocked month. Significant deviations in (b) are highlighted by a grey outline and drawn in dark colors while non-significant deviations are shown in light colors. The Euro-Atlantic and Pacific sector are highlighted by the red dashed wedges and the position of the jet stream in ERA-Interim is denoted by the blue contour (23 m s^{-1} isotach on 300 hPa) in (b). Black contours in both figures denote mean absolute blocking frequencies in ERA-Interim (contour interval of 2.5 %).
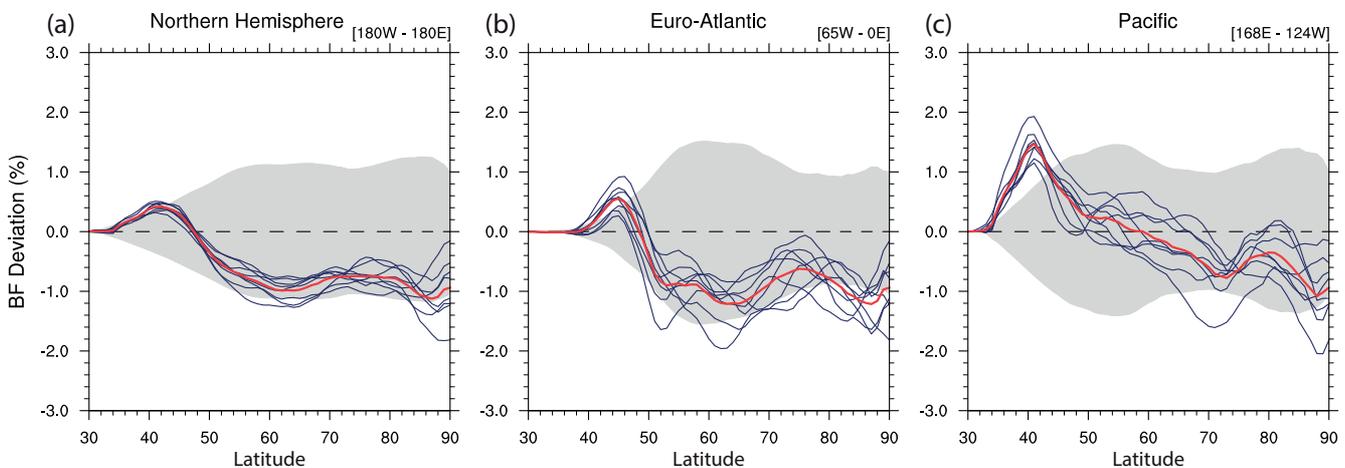
Figure 2: Annual mean, zonally averaged APV* blocking frequency deviation from ERA-Interim for the NH (a), EA (b), and PAC sector (c). The red line denotes the ensemble mean and individual members are shown as thin dark blue lines. The light grey area highlights the 2.5 to 97.5 percentile confidence interval of the ERA-Interim mean.

son (slightly higher frequencies of 16 % are only observed during autumn). A stronger seasonal cycle is found in the PAC sector with highest blocking activity in autumn (13 %) and markedly lower frequencies during summer (9 %). Conversely, the center of maximum blocking frequency does not migrate notably in the PAC sector, while the EA blocking peak describes a distinct seasonal cycle: Blocking in winter and spring is encountered more often in the central Atlantic whereas summer

and autumn events rather occur in the eastern Atlantic. Finally, the third peak of blocking activity over northern Russia is comparable in strength and location during all seasons except during summer when enhanced frequencies (exceeding 12 %) are found, together with a shift to the East Siberian Sea (130 to 180° E). Qualitatively, these findings are in line with the results from CROCI–MASPOLI et al. (2007) and SMALL et al. (2013), reporting comparable seasonal blocking occurrence. Note that
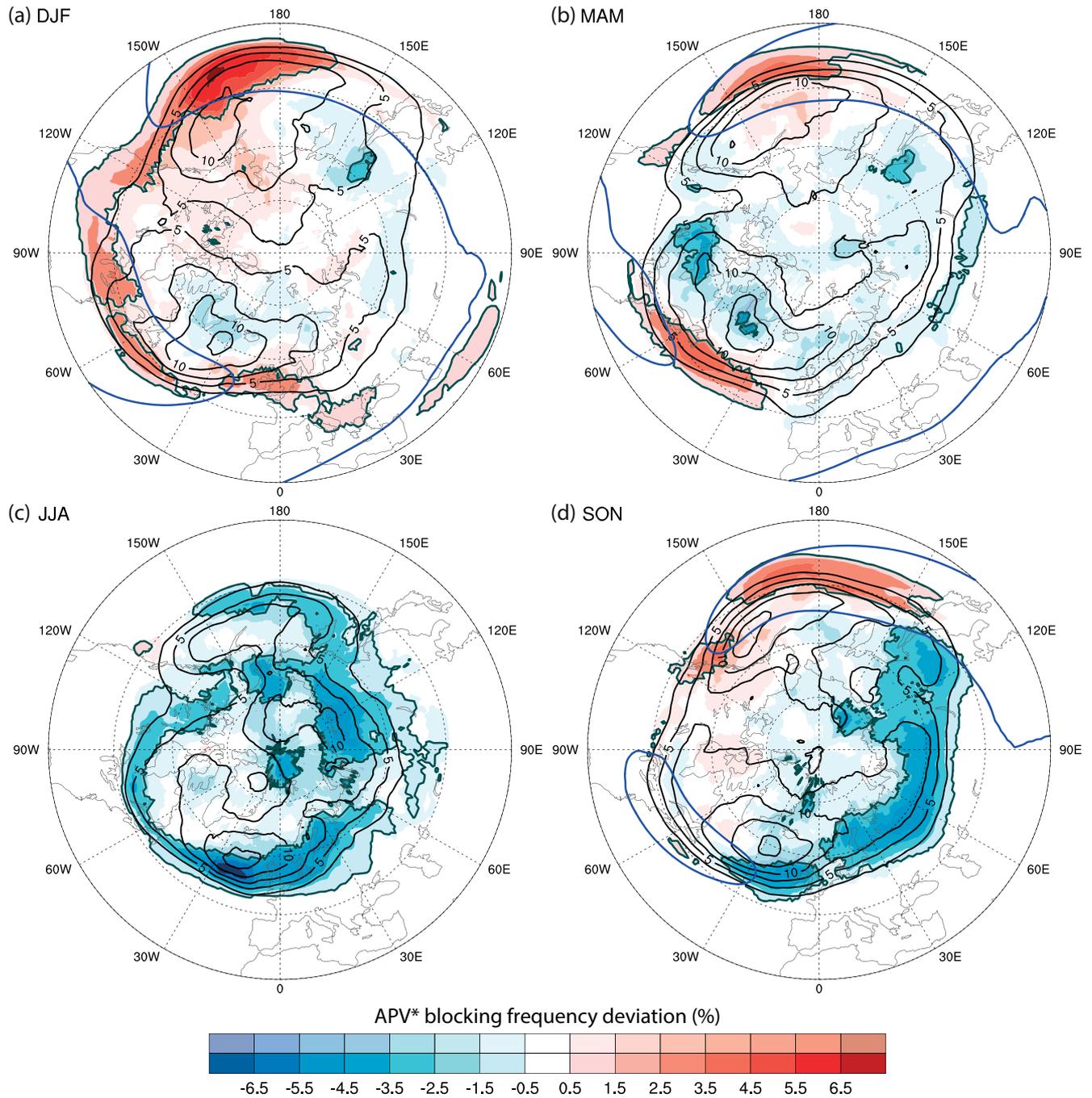
Figure 3: Seasonal APV* blocking frequency deviation from ERA-Interim during winter (a), spring (b), summer (c), and autumn (d). Significant deviations are highlighted by a grey outline and drawn in dark colors while non-significant deviations are shown in light colors. Absolute blocking frequencies (black contour with interval of 2.5 %) and the position of the jet stream in ERA-Interim are overlayed (blue contour, 23 m s^{-1} isotach on 300 hPa).

an investigation of annual and seasonal blocking occurrence over the entire ERA-Interim period revealed no significant trends using a t-test at the 5 % confidence level (not shown).

ICON is able to capture the seasonality in intensity and geographical location of the main blocking centers (shading in Fig. 3). Distinct deviations from reanalysis are mainly found at the southern flanks of high blocking activity in the mid-latitudes, where blocking occurrence is lower. During winter (Fig. 3a), an increase of

more than 5 % is observed across a large region in the mid-latitude PAC sector. With the exception of increased blocking activity (by 1 %) in the region of the Atlantic storm track, all other regions show good agreement with ERA-Interim. For spring (Fig. 3b), two regions of blocking overestimation on the order of 3 % along both the Pacific and Atlantic storm track stand out. Good agreement with ERA-Interim is found across the remainder of the Northern Hemisphere, albeit showing a tendency towards too low blocking occurrence over the Atlantic.
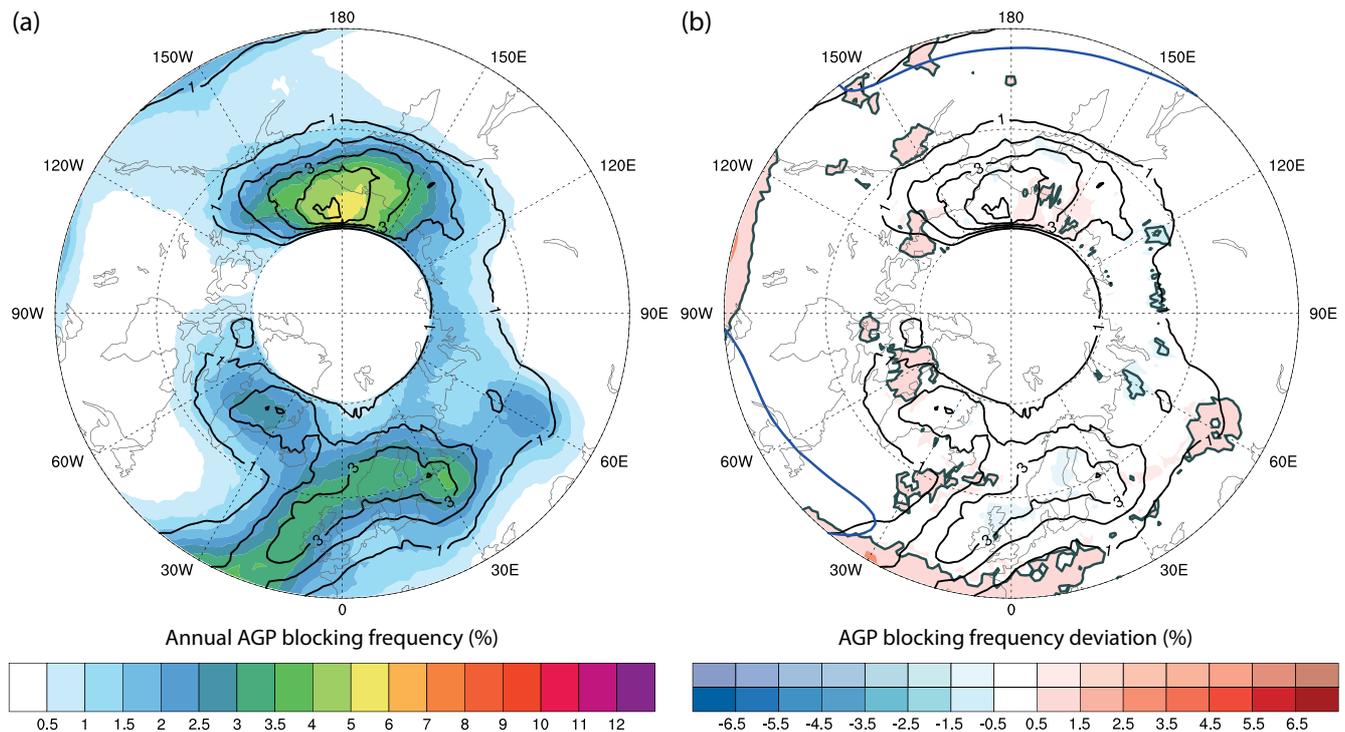
Figure 4: As Fig. 1, but for the AGP blocking index. Note that the region depicted only ranges from 45° N to the pole.

A much different picture emerges in summer (Fig. 3c) where large regions of decreased blocking occurrence are found in ICON. Most notably, a lack of blocking is observed just south of the EA blocking maxima and over Eurasia. Finally, during autumn (Fig. 3d), an increase in blocking in the region of the Pacific jet is observed, while the entire mid-latitude EA and Russian region are underestimated.

3.2 AGP blocking climatology

The annual blocking frequency distribution as identified by the AGP index is shown in Fig. 4a. Inherent to the different approach to identify blocking, partly differing blocking patterns and frequencies result. The often reported maxima of blocking activity over Northern Europe, Greenland and at the very northern tip of the Pacific ocean (e.g. ANSTEY et al., 2013; MASATO et al., 2013; SCHIEMANN et al., 2017) are reproduced in ICON. Unlike with the APV* index, no peak of blocking activity is identified at the end of the Pacific storm track. Compared with ERA-Interim, annual AGP blocking occurrence is well represented in ICON (Fig. 4b).

The spatial pattern of AGP blocking activity remains similar during all seasons except during summer, when a shift of European blocking to the north, a marked decrease over the British Isles and Norway, and a second peak of high latitude blocking over the Pacific is found (black contours in Fig. 5). Considering the deviation from reanalysis (shading), good agreement of the spatial blocking pattern is found.

Contrasting our previous findings using the APV* index, regions of AGP blocking deviations are mainly collocated with regions of maximum blocking occurrence

instead of being confined to their southern flank. During winter (Fig. 5a), a significant decrease (by about 3 %) in blocking activity is found across northern Europe. This deficit has been observed in many different models (e.g. SCAIFE et al., 2010; ANSTEY et al., 2013; SCHIEMANN et al., 2017; DAVINI et al., 2017) and is commonly attributed to the coarse resolution of the underlying simulation. It is likely that the relatively low resolution (80 km) of the model simulations contributes to this blocking bias. However, investigating the sensitivity to resolution is not within the scope of the present study. In spring (Fig. 5b), both the Pacific and Greenland blocking maxima are overestimated (by about 3 %), while blocking frequencies across northern Europe are in good agreement with reanalysis. A slight underestimation is found in all three regions of maximum blocking activity during summer (Fig. 5c). Finally, good simulation of blocking is observed in autumn (Fig. 5d), except for a slight tendency to overestimate blocking across northern Europe.

When compared with results from previous studies that adopt a flow reversal index to assess blocking in GCMs, we find that ICON performs similar to models at intermediate (~ 80 km) resolution. Blocking activity in the Euro-Atlantic region during winter is underestimated by about 50 % in ICON, which is comparable to the blocking bias observed across Coupled Model Intercomparison Project (CMIP5) models (MASATO et al., 2013). In contrast, blocking in summer is generally better simulated in ICON than by most CMIP5 simulations. The representation of blocking during spring is comparable with the high resolution (T1279) simulation of the IFS (Integrated Forecast System) as described by
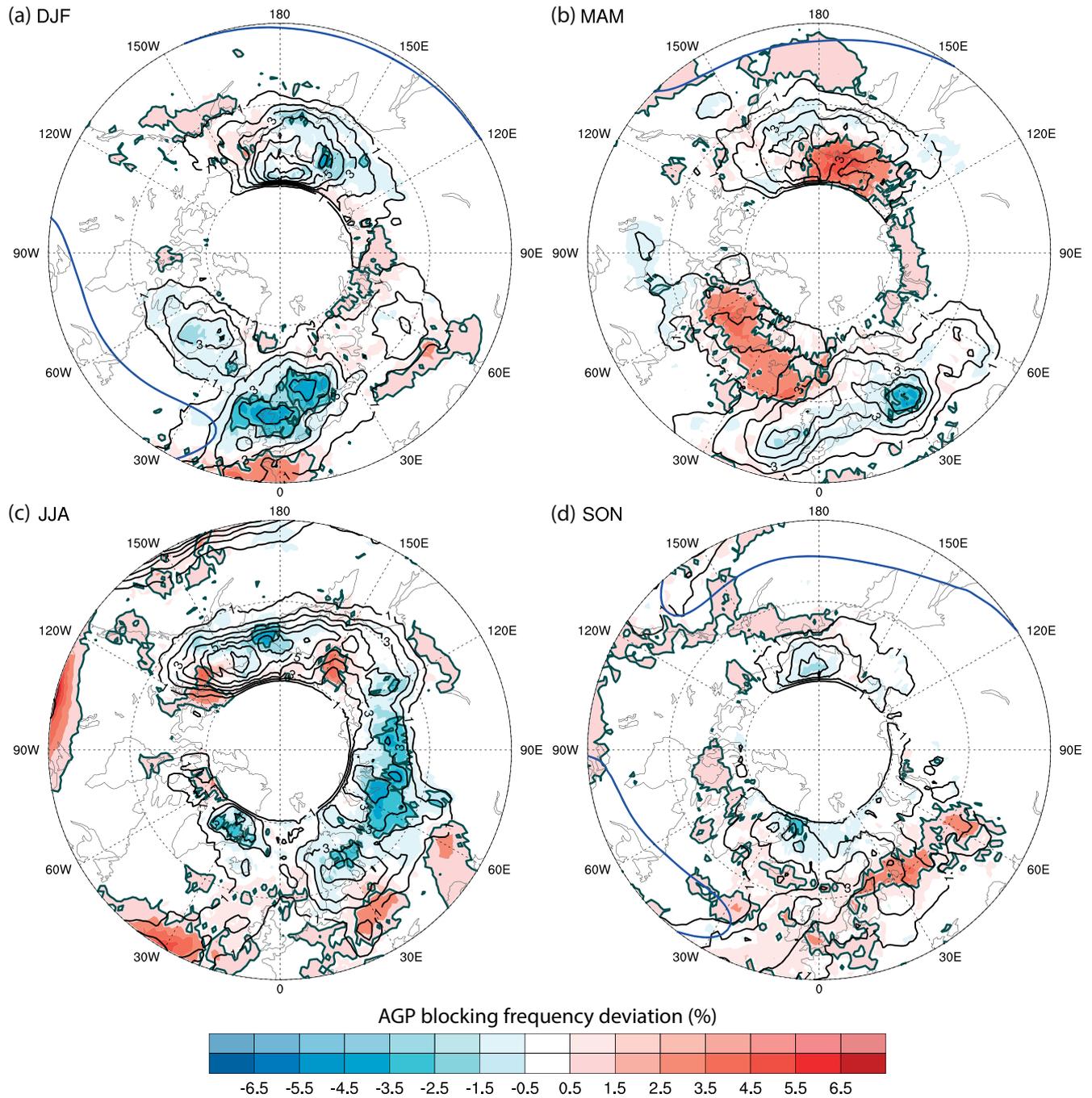
(a) DJF

(b) MAM

(c) JJA

(d) SON

AGP blocking frequency deviation (%)

-6.5   -5.5   -4.5   -3.5   -2.5   -1.5   -0.5   0.5   1.5   2.5   3.5   4.5   5.5   6.5

Figure 5: Seasonal AGP blocking frequency deviation from ERA-Interim for winter (a), spring (b), summer (c), and autumn (d). Significant deviations are highlighted by a grey outline and drawn in dark colors while non-significant deviations are shown in light colors. Absolute blocking frequencies (black contour with interval of 1 %) and the position of the jet stream in ERA-Interim are overlayed (blue contour, 23 m s⁻¹ isotach on 300 hPa). Note that the region depicted only ranges from 45° N to the pole.

SCHIEMANN et al. (2017). Finally, similar blocking frequencies as those simulated by the MRI (Meteorological Research Institute) model at roughly 63 km resolution (TL319) are found in autumn (SCHIEMANN et al., 2017).

While the underestimation of blocking in the Euro-Atlantic region is an interesting feature described by the AGP blocking index, we argue that the identified blocking activity in the Pacific sector requires careful interpretation. Blocking in the eastern Pacific usually adopts an omega-shape as opposed to the classical dipole-shape,

which is more frequent in the Euro-Atlantic region (e.g. ALTENHOFF et al., 2008). Omega-blocks are characterized by an open ridge structure and are usually not associated with wave breaking (SUMNER, 1954). Therefore, no significant reversal of the geopotential height gradient occurs, rendering omega blocks difficult to detect by the AGP index (BARRIOPEDRO et al., 2010). For this reason, no counterpart of the European mid-latitude blocking maxima is found in the Pacific region (Fig. 5). However, because blocking is inherently linked to transient

eddies as well as wave breaking, increased blocking occurrence at the end of both storm tracks, as observed with the APV* index (Fig. 3), is expected.

In summary, while both indices show reasonable representation of blocking in ICON, a direct comparison between the observed blocking frequency deviations is not possible. Because the APV* index is able to identify both dipole- and omega-shaped blocks and since more pronounced deviations from ERA-Interim occur, we focus further investigations on potential causes for seasonal APV* blocking deviations. Namely, we investigate (i) the overestimation of blocking in the PAC region during winter, (ii) the increased frequencies in the region of the Pacific and Atlantic storm track in spring, and (iii) the decreased blocking frequencies in the EA domain during summer and autumn. Note that, if not otherwise stated, blocking is described as identified by the APV* index in the following.

3.3 Blocking characteristics

Potential causes for the identified blocking deviations are explored by comparing blocking characteristics in ICON with those from ERA-Interim (Fig. 6). To this end, for each individual blocking event, information regarding its center of mass, duration, size, intensity as well as climatological VAPV in the blocked region is computed. Blocking duration describes the lifetime (in days) from the first to the last time of identification by the blocking diagnostic. Blocking size (in km^2) is defined as the spatial extent of the region exceeding the anomaly criterion. Blocking intensity (in PVU) and climatological VAPV (in PVU) are defined as the area-weighted negative VAPV anomaly and VAPV climatology, respectively, in the blocked region. The latter three characteristics (blocking size, intensity, and climatological VAPV) are temporal averages over the entire life cycle of the respective block. Each blocking event is affiliated to a specific region by requiring its center of mass to fall into one of the sectors considered for at least 50 % of the blocks lifetime. Moreover, each blocking event is assigned to the season of onset. When comparing results from ICON (red dots) with reanalysis (box plots) in the following, we relate to the average blocking characteristic derived from the ICON ensemble mean and the distribution obtained from a 1000 trial Monte Carlo resampling of ERA-Interim metrics.

A distinct seasonal cycle is observed regarding the area occupied by blocks (Fig. 6a). On average, their size range from 1.6×10^6 km^2 in summer to 2.4×10^6 km^2 during winter, the latter roughly corresponding to the size of Greenland. This variance in size is consistent with the fact that the tropopause is at a higher altitude in summer. Thus, at a fixed latitude, climatological VAPV values are generally reduced in summer, which leads to a decrease in the area exceeding the negative PV anomaly required by the blocking diagnostic (considering a feature of identical instantaneous VAPV as

in winter). Events occurring in the EA (Fig. 6b) and PAC (Fig. 6c) domain describe a similar seasonal cycle, however winter blocks are on average 0.33×10^6 km^2 larger than the northern hemispheric mean. Similar variations are found by SMALL et al. (2013), albeit they reported roughly twice the size in all regions. This can be attributed to their choice of a higher cutoff value required for the blocking identification (-1.0 instead of -1.3 PVU as used in this study). The seasonal cycle is qualitatively well captured in ICON. However, blocking tends to be too small, particularly in summer when blocks are on average 0.26×10^6 km^2 smaller.

Information about blocking duration is presented in the second row of Fig. 6. On average, blocking lasts for 10 to 11 days. No consistent seasonal cycle is observed regarding the entire NH and the PAC region. However, a marked decrease in the duration of EA blocks is found during spring. This decrease is not evident in ICON, i.e. the seasonal variability of blocking duration is not simulated well by the model in the EA region. Furthermore, ICON consistently underestimates blocking duration in summer. In general, ICON tends to produce blocking events of insufficient persistence, except during autumn in the PAC domain and during spring in the EA region.

The third row of Fig. 6 shows the average number of blocking events in each sector and season. Regarding the NH and the EA sector, the fewest events are observed during winter. While this appears to be in contradiction with the seasonal blocking frequency distribution previously shown (higher frequencies in winter than during summer, Fig. 3), winter blocks are on average 1×10^6 km^2 larger thus compensating for the lack of events. The number of events occurring in the PAC sector are less dependent on the season considered. Overall, ICON tends to overestimate the number of blocking events throughout all seasons and regions. This is especially noticeable during winter where on average 3 more events occur in ICON across the entire NH and about 1 more block is observed in the EA and PAC region.

Further, we investigate the climatological VAPV in the blocked region (Figs. 6j–l). This metric relates to the background VAPV used for the anomaly computation and indicates PV mean state biases near the tropopause. A weak seasonal cycle is evident in ERA-Interim, with higher values during spring and summer than in autumn and winter. This is surprising, as the tropopause is generally located higher in summer than in winter, which should reduce VAPV at a fixed latitude (VAPV is calculated between 500 and 150 hPa all year). On the other hand, since blocking is expected to roughly follow the north–south oscillation of the jet stream, this metric indicates that summertime blocks are generally located much further to the north (where the tropopause becomes lower) than their wintertime counterparts. Qualitatively, the seasonal cycle is well represented in ICON, however all regions and seasons show a systematic bias towards lower VAPV values, indicating that the tropopause is at a higher altitude (except for the EA sector during winter). We argue that this robust decrease in
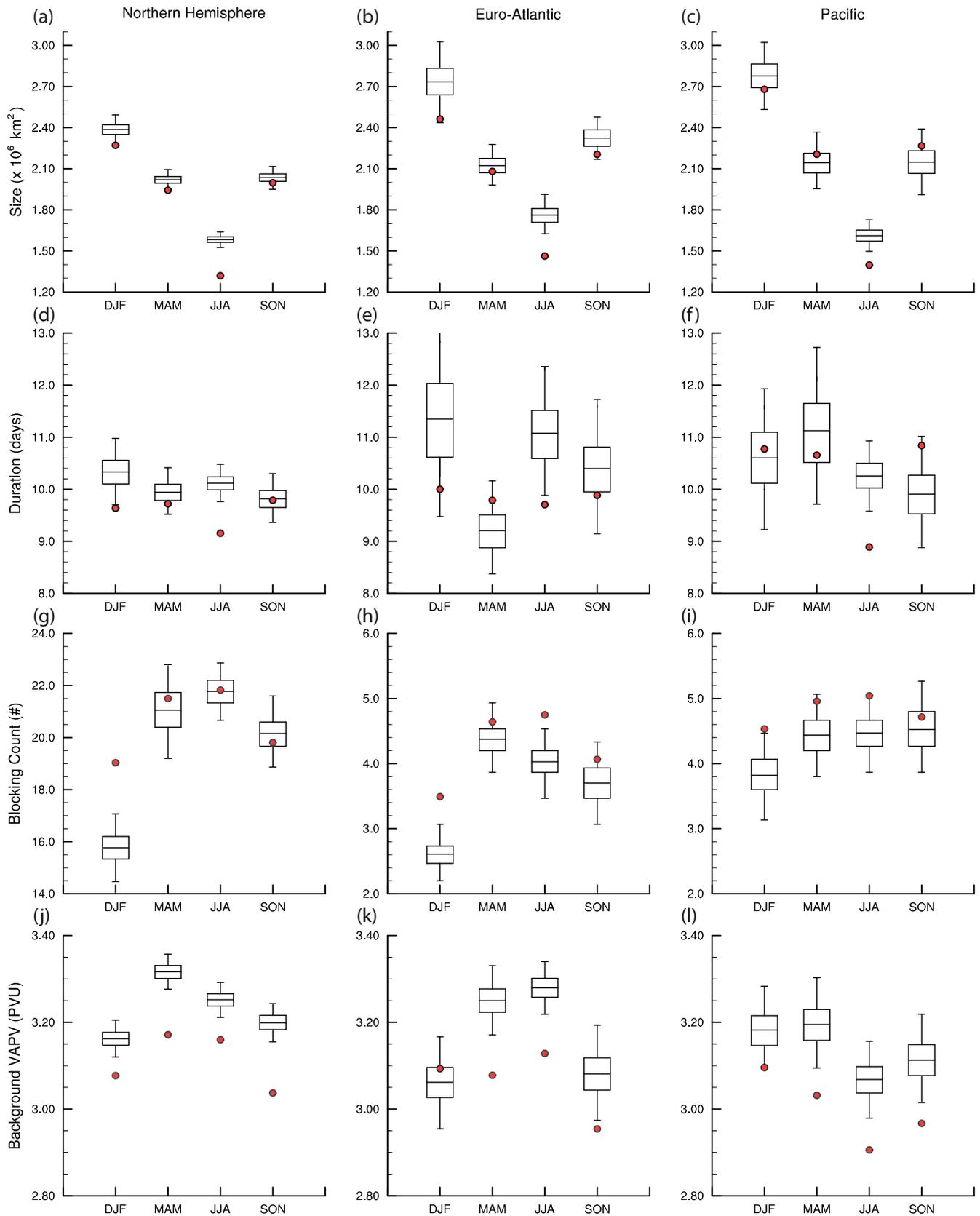
Figure 6: APV* blocking characteristics in ERA-Interim (boxes) and ICON (red dots) for the Northern Hemisphere (a,d,g,j), the EA (b,e,h,k), and PAC region (c,f,i,l). Shown are blocking size (a–c), duration (d–f), number of blocking events (g–i), and climatological VAPV in the blocked region (j–l). The boxplots depict the 2.5 to 97.5 percentile (whiskers) and interquartile range (box) together with the overall mean (horizontal line) derived from Monte Carlo re-sampling of ERA-Interim characteristics. Points outside the whiskers describe statistically significant deviations of the respective metric from ERA-Interim.
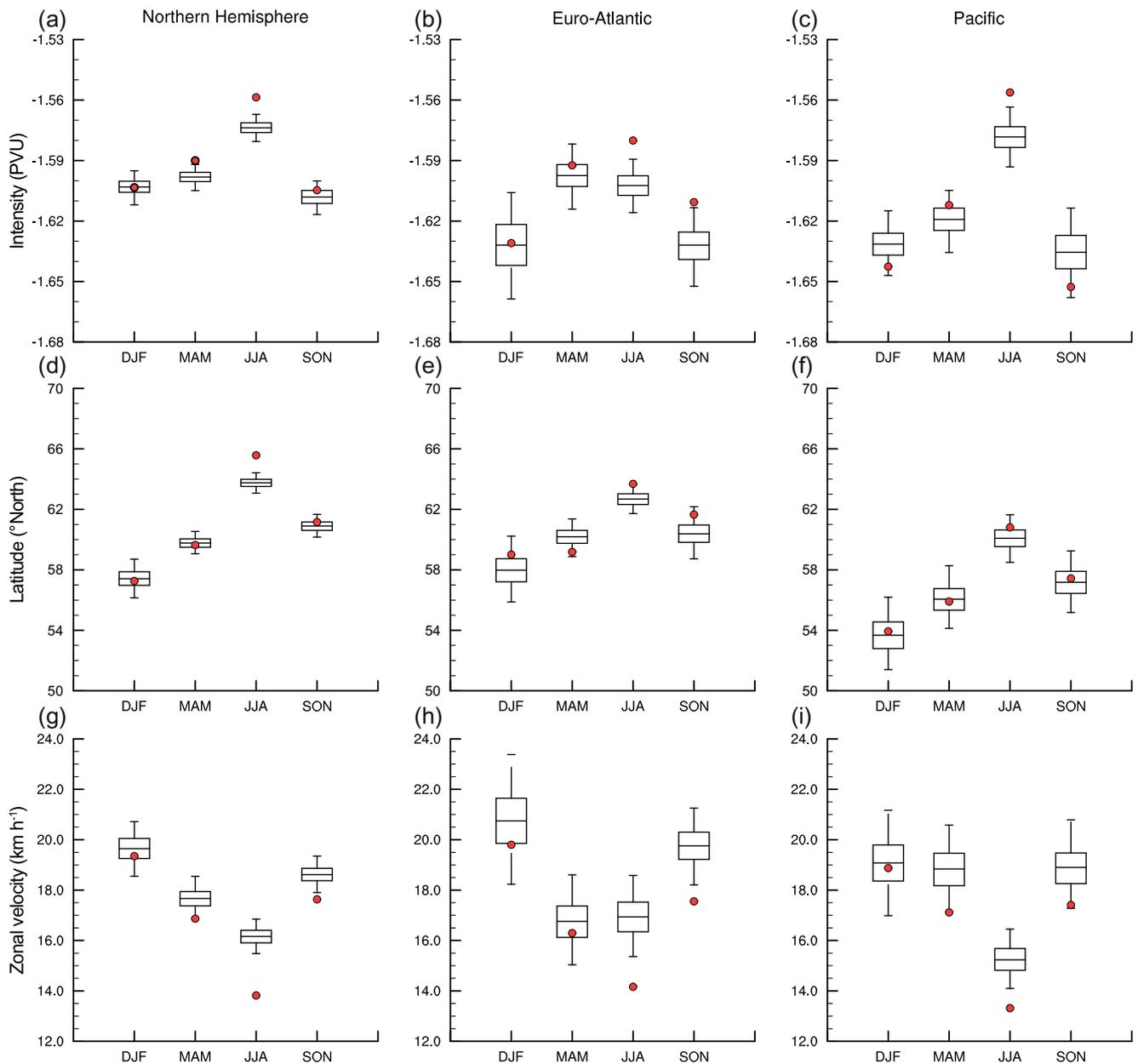
Figure 7: As Fig. 6, but for intensity (a–c), latitude (d–f), and zonal velocity (g–i).

VAPV is closely linked to the systematic underestimation of blocking size (Figs. 6a–c), since a smaller area will exceed the threshold required for the anomaly based blocking index, when considering a block of identical intensity. The origin of this mismatch will be investigated in Section 4.2.

Regarding blocking intensity (Figs. 7a–c), no marked seasonal cycle is apparent in ERA-Interim, however blocking events are significantly weaker (i.e. the anomaly is less negative) during summer compared to the other seasons. ICON correctly captures the seasonal variation in intensity except during summer when blocking strength is underestimated. This is consistent with the fact that both background VAPV (Figs. 6j–l) and blocking size (Figs. 6a–c) are underestimated in ICON. To elucidate our finding that blocking events generally occur in a higher VAPV background in summer than during winter, we also consider the latitudinal position of blocks (Figs. 7d–f). A distinct seasonal cycle is observed in reanalysis, with summertime events being located more northerly indeed (on average at 64° N) than winter blocks (on average at 57° N). Thus, blocking events roughly follow the jet stream and are located in an environment of decreased tropopause height and thereby increased VAPV in summer. While blocks occur more northerly in ICON during summer, no deviation from reanalysis is found during the other seasons. Therefore, their position can not account for the marked decrease in background VAPV (Figs. 6j–l). Finally, a distinct seasonal cycle is found regarding the zonal displacement speed, with higher velocities during winter than summer (Figs. 7g–i). ICON agrees well with ERA-Interim except during summer when a robust decrease in speed is found, attributable to the decrease in blocking duration.

A remark on the definition of blocking as quasi-stationary features is made here. The zonal velocity discussed above is only a rough estimate of the actual zonal displacement of a block. Spurious shifts in the location of the center of mass (i.e. broadly the region where the PV anomaly is strongest) lead to artificial peaks in the apparent displacement. When considering the criterion invoked to ensure quasi-stationary in other studies, which usually consists of a restriction on the maximum allowed longitudinal displacement per day (BERCKMANS et al., 2013,), similar velocities result. Therefore, the criterion of 70 % overlap between two 6-hourly time steps is sufficient to distinguish stationary blocks from transient eddies.

Using the information gained from the study of blocking characteristics in ICON, we summarize that (i) most blocking characteristics compare well with ERA-Interim. However, blocking duration appears to be insensitive to the season and region of blocking occurrence (Figs. 6d–f). This hints towards issues regarding the maintenance of blocking in ICON. (ii) Blocking generally occurs too often in the model (Fig. 6g), which might indicate a misrepresentation of the processes leading to blocking. (iii) The underestimation of size and duration likely plays a key role for the decreased blocking occurrence across the entire NH during summer in ICON (Fig. 3c). What forces this bias is investigated in Section 4.1. (iv) Since no distinct deviation from reanalysis in terms of blocking characteristics are found in the PAC domain during spring, other causes for the overestimation of blocking in that region (Fig. 3b) are explored in Section 4.2. (v) The increase in the number of blocking events in the PAC region during winter (on average 0.7 more per season than in ERA-Interim) likely plays a key role in producing the reported blocking overestimation (Fig. 3a).

4 Influence of the mean state

Blocking is identified as a region of anomalously low upper-level VAPV when compared against the monthly VAPV climatology (see Section 2.2). A region of increased climatological VAPV is thus more favourable for blocking to be identified, since higher instantaneous VAPV values (i.e. weaker blocking events) are sufficient to exceed the required VAPV anomaly threshold (≤ -1.3 PVU). This generally results in larger and more negative VAPV anomalies. Conversely, it is more difficult to detect blocking occurring in a region of reduced climatological VAPV, since lower VAPV values (i.e. stronger blocking events) are required to exceed the anomaly threshold. Low climatological VAPV thus force smaller and weaker VAPV anomalies. Therefore, biases in the model's mean state can result in an erroneous (non-)identification of blocking and a modulation of blocking characteristics. In this section, we explore how this process can explain a selected number of observed deviations in blocking occurrence and blocking characteristics.

4.1 Mean state biases

Complementing the assessment of blocking in ICON, the climatological deviation of PV, TH, and the zonal wind from ERA-Interim as well as the deviation of Qv from MLS measurements are examined using seasonal, zonally averaged cross-sections for the PAC region during winter (Figs. 8a–c) and spring (Figs. 8d–f) and for the EA sector during summer (Figs. 8g–i). We only show these regions and seasons because no additional insight could be gained from the other combinations.

Beginning with winter, we find that the tropospheric distribution of PV in the PAC domain (Fig. 8a) is almost identical to ERA-Interim. In the lower stratosphere, a PV dipole with decreased values of PV (by about 0.3 PVU) in the vicinity of the tropopause is observed, explaining the slight increase in the tropopause height (green vs. black line). Note that the PV dipole covers the upper part of the column for which VAPV and consequently VAPV anomalies are computed (500–150 hPa), which potentially influences blocking identification. In terms of TH, a negative bias of -4 K is observed at a height of 200 hPa (Fig. 8b). Following the definition of PV (e.g. HOSKINS et al., 1985), differences therein must be proportional to the vertical gradient of the difference in TH. Therefore, we expect a negative PV anomaly below the negative TH anomaly and a positive PV anomaly aloft, as seen when comparing Fig. 8a with Fig. 8b. The PV dipole in ICON is thus directly linked to a lower stratospheric cold bias. Moreover, an upward and poleward shift of the subtropical jet stream is found producing an anticyclonic wind anomaly (Fig. 8c). This explains the large negative PV bias encompassing the entire stratosphere between 30° and 40° N. A comparison of specific humidity in ICON with water vapour measurements from the MLS satellite revealed no distinct deviations (Fig. 9a).

The aforementioned PV dipole is strengthened during spring (Fig. 8d), thereby considerably elevating the tropopause between 45° and 75° N. In contrast, a region of increased PV encompasses the entire tropopause between 35° and 42° N. This increase in PV locally lowers the dynamical tropopause (at 35° N) and induces a cyclonic wind field, resulting in a southward shift of the subtropical jet (Fig. 8f). A negative TH anomaly of -6 K is observed at 200 hPa (Fig. 8e), explaining the PV dipole. Regarding the distribution of specific humidity, a region of increased moisture on the order of 1.6 times the regular values is found at around 200 hPa (Fig. 9b).

Finally, focusing on the mean state in the Euro-Atlantic region during summer, a pronounced PV dipole is observed across the lower stratosphere and upper troposphere (Fig. 8g). The strong decrease in PV at the tropopause results in a marked raise thereof. A remarkable negative temperature bias exceeding -8 K is again observed at a height of 200 hPa (Fig. 8h) and is responsible for the biases in the PV mean state. A slight weakening of the subtropical jet is found (Fig. 8i), po-
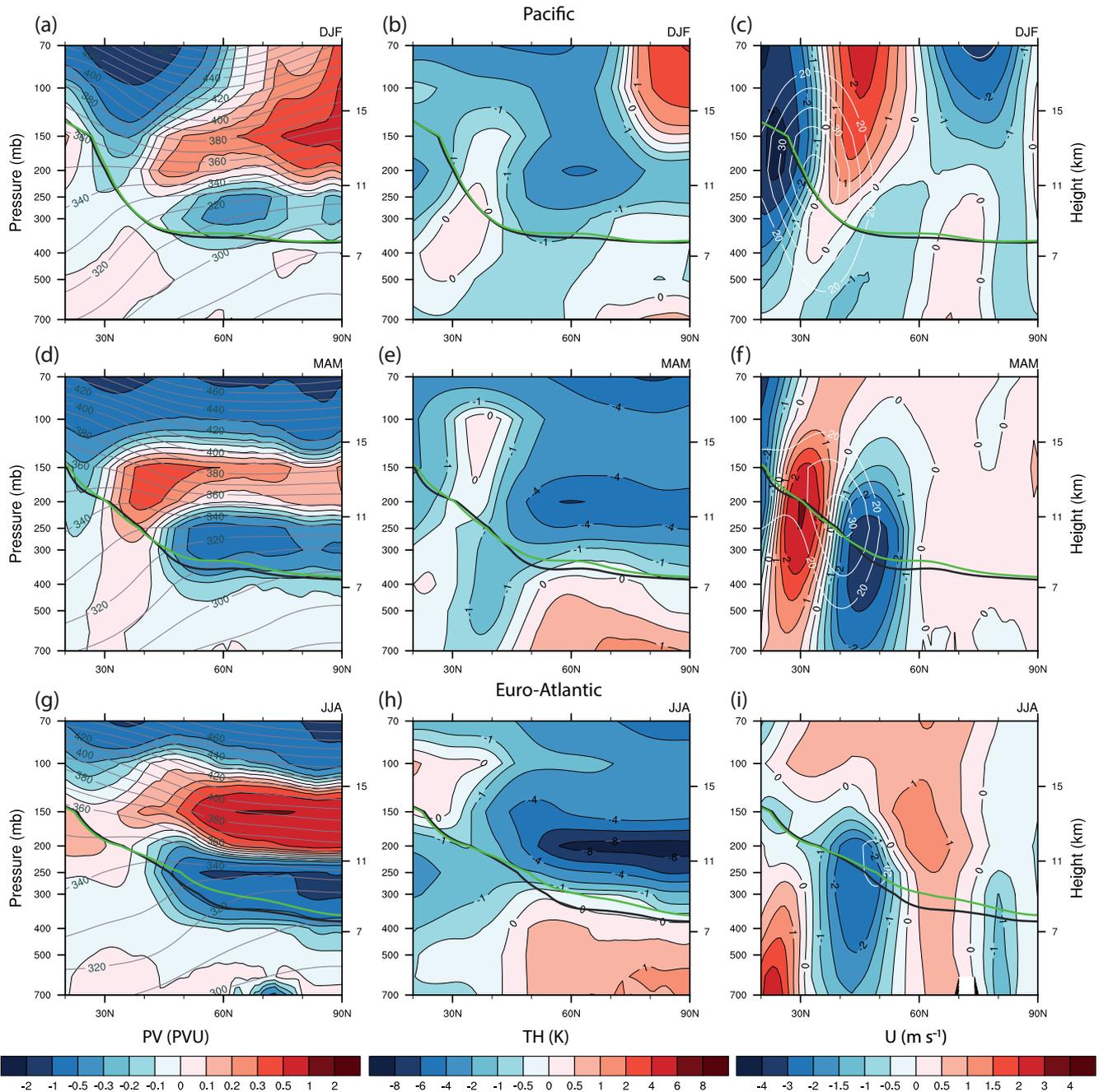
Figure 8: Cross-sections of zonally averaged PV, TH, and zonal wind deviations from ERA-Interim for winter (a–c), spring (d–f), and summer (g–i). Panels (a–f) depict the Pacific region while (g–i) show the Euro-Atlantic sector. The dynamical tropopause (2 PVU isoline) in ICON (green) and ERA-Interim (black line) are overlaid. Seasonal means of TH (contour interval of 10 K) in (a,d,g) and zonal wind (isotachs at 5 m s⁻¹ intervals) in (c,f,i) are derived from ERA-Interim. Note the nonlinear color scales.

tentially owing to the decreased baroclinicity at low levels which is linked, via thermal wind balance, to jet strength (indicated by the positive low-level TH anomaly at the pole and the negative anomaly towards the equator). A strong overestimation of lower stratospheric specific moisture (reaching almost 3 times the observed values at 200 hPa) is observed when comparing ICON with a climatology of MLS satellite measurements (Fig. 9c). Owing to the increased water vapour concentration above the tropopause, a region of intense radiative cooling exists in the lower stratosphere where

specific humidity eventually decreases with height, producing the observed cold bias and thereby lifting the dynamical tropopause. STENKE et al. (2008) found a similar behaviour in ECHAM4 simulations and attributed the increase in moisture to numerical diffusion of water vapour across the tropopause.

From these observations, we can draw a few conclusions regarding the influence of the mean state on blocking identification and characteristics in ICON. The ubiquitous decrease in PV in the vicinity of the tropopause north of 50° N reduces the area that exceeds
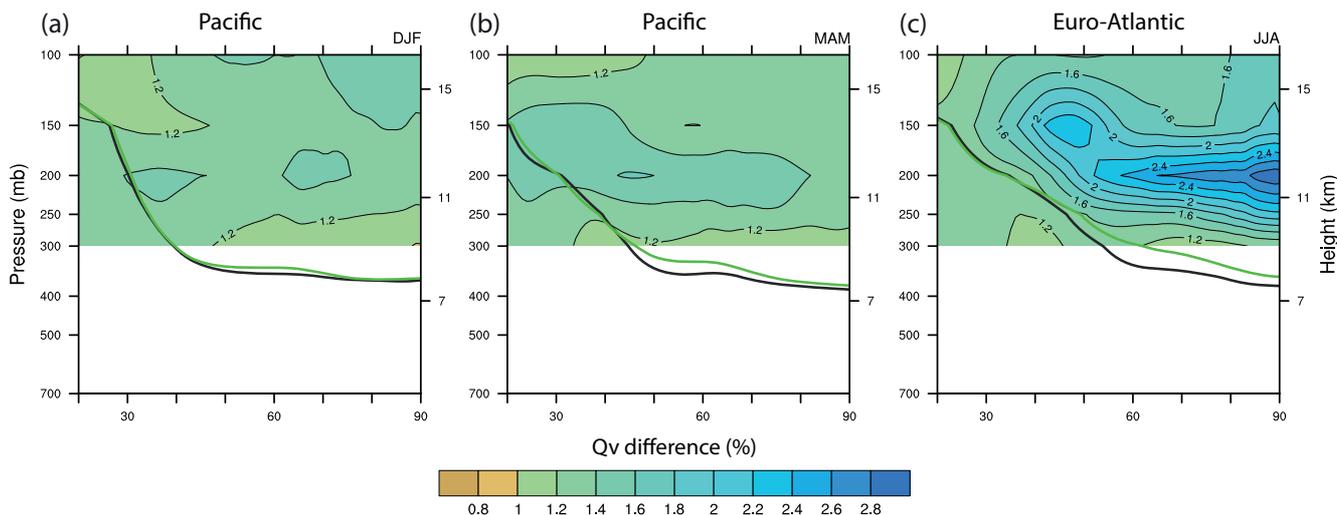
Figure 9: Cross-sections of zonally averaged specific humidity deviations from MLS measurements in the Pacific region for winter (a) and spring (b) and in the Euro-Atlantic sector for summer (c). The dynamical tropopause (2 PVU isoline) in ICON (green) and ERA-Interim (black line) are overlaid. Note that the satellite measurements are unreliable below 300 hPa (Waters et al., 2006) and have therefore been omitted.

the threshold required for the anomaly based blocking identification which explains the decrease in blocking size (Figs. 6a–c). The PV bias further explains the significant decrease in background climatological VAPV during all seasons and sectors (Figs. 6j–l). The decrease in PV at tropopause level is linked to a cold bias in the lower stratosphere, likely resulting from the overestimation of lower stratospheric moisture. However, the good representation of the mean state during winter in the PAC sector is in stark contrast to the strong blocking overestimation reported in Fig. 3a. Therefore, dynamical processes must be responsible for this observed increase in blocking activity, rather than an erroneous identification due to mean state biases. The increase in PV at roughly 35° N in the Pacific sector during spring enhances the potential for blocking to be identified in this domain (as found in Fig. 3b). Finally, the very strong decrease in PV at tropopause height during summer in the EA region leads to a marked decrease in blocking size and duration as reported in Fig. 6b,e as well as intensity (Fig. 7b).

4.2 Sensitivity of blocking identification to the mean state

In order to support our previous findings and to further explore the impact of the mean state on blocking identification, we introduce a measure to distinguish between regions that are influenced by a biased mean state from regions that are more influenced by an actual, dynamically motivated modulation of blocking activity. This is achieved by correcting the PV mean state bias in the model before applying the blocking index, similar to the approach chosen by Scaife et al. (2010) to disentangle the effect of enhanced zonality on blocking identification in the reversal based blocking framework. To this

end, we re-computed VAPV anomalies in ICON using monthly VAPV climatologies based on ERA-Interim. The resulting blocking distribution (BF2 in the following) is therefore unbiased in terms of the mean state. By subtracting BF2 from the regular blocking frequencies (BF1, which contain deviations due to both the dynamics and the mean state) we obtain a measure for the influence of the mean state on blocking identification. Note that explaining the physical drivers leading to an increase or decrease of blocking in ICON is not within the scope of the present study.

Fig. 10 shows the results of this investigation for three seasons. The first column displays regular blocking frequency deviations from ERA-Interim as discussed before (BF1, cf. Fig. 3). The second column shows the deviation of the VAPV climatology from reanalysis and the third column contains the measure for the influence of the mean state on blocking (i.e. BF1 −BF2). For winter, we find that in the region of significantly increased blocking frequencies over the Pacific ocean (marked region in Fig. 10a), no deviation of the climatological VAPV distribution is found (corroborating Fig. 8a). By construction, no signal results in Fig. 10c. This emphasizes the importance of dynamical processes in producing the overestimation of blocking in this region.

A different picture emerges during spring. An area of increased blocking frequencies is found over the midlatitude Pacific region (Fig. 10d). The same region is characterized by a significant increase in climatological VAPV (Fig. 10e) leading to an increase in blocking frequency due to the mean state bias (Fig. 10f). As the strength of this signal is comparable to the total blocking frequency error (marked region in Fig. 10d), we argue that this feature describes an erroneous increase in identified blocks instead of an actual overestimation of blocking in ICON. Focusing on the mid-latitude EA do-
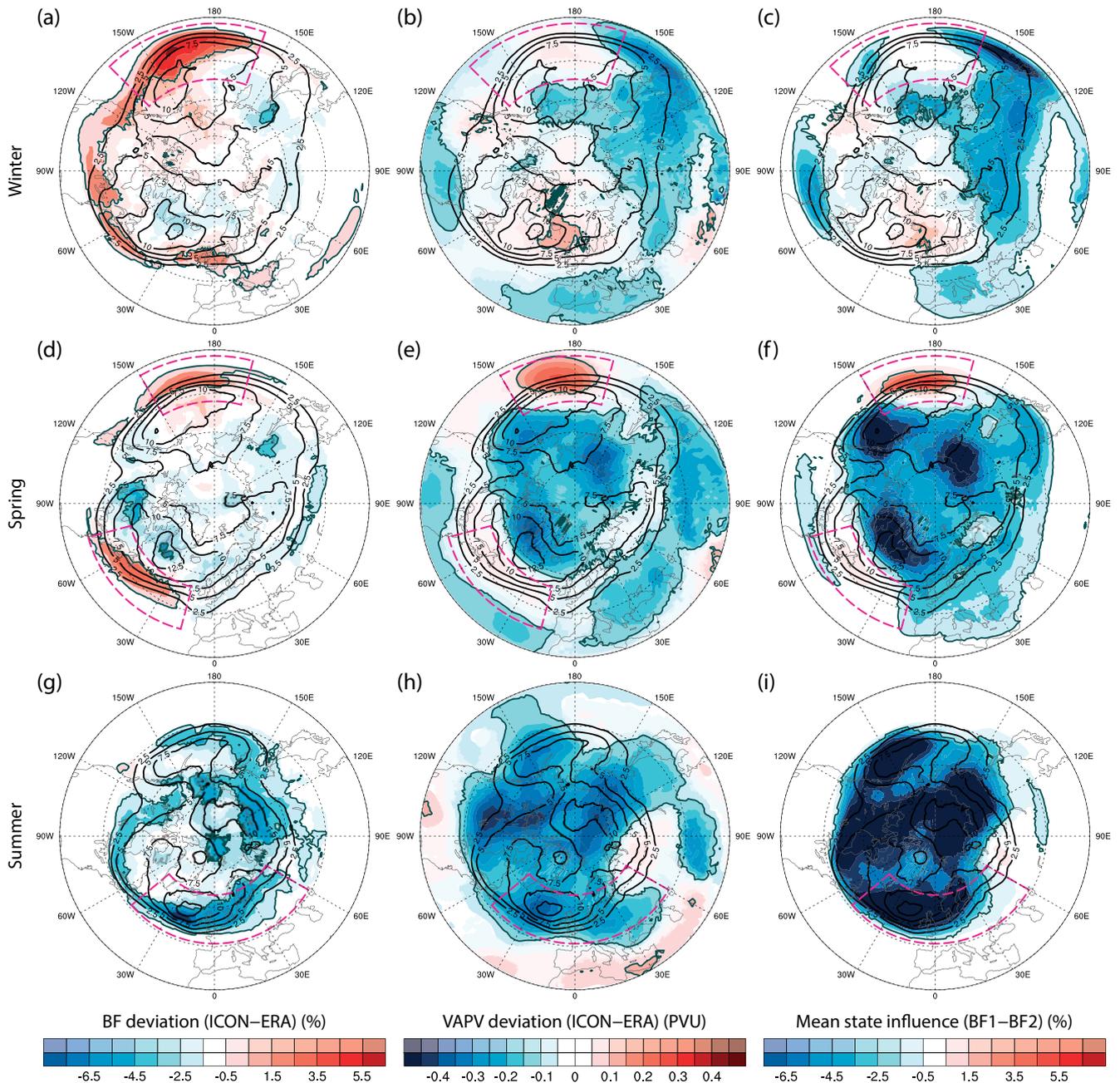
Figure 10: APV* blocking frequency deviations from ERA-Interim (a,d,g), deviations of the VAPV climatology (b,e,h), and the influence of the mean state on blocking (c,f,i) for winter (a–c), spring (d–f), and summer (g–i). Significant regions are highlighted by a grey outline and drawn in dark colors while non-significant deviations are shown in light colors. Black contours indicate absolute blocking frequencies in ERA-Interim and regions of interest are marked by purple boxes.

main, blocking is also overestimated (Fig. 10d). However, no clear signal in the mean state bias (Fig. 10e,f) is observed, indicating the relevance of dynamical processes in forcing the increase in blocking occurrence in the EA sector during spring. On the other hand, three regions of significantly decreased VAPV and consequently mean state influence are found where blocking occurrence appears to agree well with ERA-Interim. It is likely that ICON effectively overestimates blocking in these regions, leading to a decrease in climatological VAPV (as blocks are associated with low-PV) and

thereby decreasing the size and intensity of identified blocks.

When repeating the same analysis for summer, vast regions of the NH are characterized by decreased VAPV (Fig. 10h). Consequently, the mean state exerts a strong influence on blocking identification (Fig. 10i). The mean state bias strongly modulates blocking characteristics across all regions during summer (Section 4.1) and drives the underestimation of blocking in the midlatitudes, especially in the EA sector. However, since the mean state signal (Fig. 10i) is much stronger than the ap-

parent underestimation of blocking (Fig. 10g), it is difficult to disentangle the exact influence that the mean state and the model's dynamics exert on blocking occurrence.

In summarizing, we find that mean state biases in ICON have the potential to significantly affect the identification and characteristics of blocking in the anomaly framework. This is especially evident during summer and over the Pacific in spring, where a large fraction of the observed error can be attributed to the biased mean state. Generally, the reduced upper tropospheric PV mean state decreases blocking size and intensity towards the pole. This reduction is partly forced by a lower stratospheric cold bias but could also be associated with an increase in actual blocking activity in ICON, which could effectively be masking its own signal.

5 Summary and conclusions

This study assessed the representation of atmospheric blocking in the new global non-hydrostatic NWP model ICON. An eight member ensemble, each containing 15 years of AMIP-type simulations, was compared against ERA-Interim. Blocking was identified using both an anomaly based (APV*) and a flow reversal blocking index (AGP). The first index is based on the identification of anomalously low-PV below the dynamical tropopause (SCHWIERZ et al., 2004), while the second approach identifies blocking by the reversal of the latitudinal geopotential height gradient (SCHERRER et al., 2006). The latter method revealed the often observed negative blocking bias in the Euro-Atlantic region during winter (ANSTEY et al., 2013; SCHIEMANN et al., 2017; DAVINI et al., 2017), likely driven by the comparatively low horizontal resolution of the simulation (approximately 80 km). Owing to the difficulty of the flow reversal method to identify omega-type blocking, which is often observed in the eastern Pacific (ALTENHOFF et al., 2008), no maxima at the end of the Pacific storm track was detected. Due to this limitation, further results pertain to blocking as identified by the APV* index.

The annual frequency and spatial distribution of APV* blocking is adequately simulated in ICON, with three distinct centers of action towards the end of the Pacific and Atlantic storm track, as well as over northern Russia. Deviations from ERA-Interim are confined to the mid-latitudes, most notably in the Pacific region. Considering the seasonal cycle, deviations on the order of 5 % emerge. Nevertheless, the seasonal variation in intensity and the shift in location of the main blocking regions remain well represented. Four distinct areas of deviation from reanalysis are further examined: A large region of enhanced blocking activity (> 5 %) in the Pacific domain during winter, a smaller area of increased blocking occurrence (3 %) in the region of the Pacific and Atlantic storm track during spring, and a band of underestimated frequencies (5 %) in the mid-latitudes across the Eurasian continent during summer.

A first indication of the underlying reasons for the described blocking deviations is given by assessing blocking characteristics. The most striking differences are found during summer, when blocking in ICON is characterized by decreased duration, size, and intensity, linked to a large-scale underestimation of blocking. In contrast, hardly any deviations from reanalysis are found in the Pacific region during spring. Finally, a robust increase in the number of blocking events is observed during winter. In short, deviations in blocking characteristics can only partly explain the observed differences in blocking frequencies.

Good representation of the tropospheric mean state is found during winter in the Pacific sector. A negative temperature bias is observed at about 200 hPa, forcing a decrease in PV below and an increase above. This cold bias and consequently the PV dipole is enhanced during spring, thereby lifting the tropopause north of 50° N. Conversely, a positive PV anomaly is positioned between 30° and 40° N, which lowers the tropopause height, and potentially facilitates the identification of blocking in the mid-latitude Pacific region in spring. Finally, the mean state in the Euro-Atlantic region during summer exhibits an even larger negative temperature bias in the lower stratosphere (exceeding −8 K) which leads to a marked decrease in PV at the tropopause.

A measure for the impact of mean state biases on APV* blocking identification was introduced by calculating VAPV anomalies with respect to the monthly VAPV climatology of ERA-Interim instead of ICON. This investigation reveals that the mean state has no influence on blocking in the Pacific region during winter, highlighting the importance of dynamical processes in producing the observed blocking overestimation. Conversely, a strong signal was found in the Pacific sector during spring. In line with the increased values of PV in the vicinity of the tropopause, the increased blocking occurrence in this region and season is likely an artefact of the biased mean state and not dynamically forced. On the other hand, mean state biases cannot explain the increased frequencies in the Atlantic basin during spring. Further, three areas of reduced VAPV in regions with good blocking representation are found in spring. This implies that an increase in dynamical blocking is potentially masked by a decrease in identified blocking size and intensity due to the biased mean state. Finally, the marked decrease in blocking activity across the entire NH during summer can partly be attributed to the heavily biased mean state, i.e. the reduction of PV in the upper troposphere forced by the cold bias in the stratosphere, which reduces identified blocking size and intensity. The observed temperature bias is likely the result of increased lower stratospheric specific humidity due to numerical diffusion of water vapour across the tropopause (as described for the ECHAM4 GCM by STENKE et al., 2008).

Considering the robustness of our results with respect to the choice of an anomaly based blocking index, it is apparent that mean state biases exhibit a strong influ-

ence on the identification and characteristics of blocking. A large-scale decrease in climatological upper tropospheric PV (e.g. because more blocking is present in the model) can result in an apparent reduction of the detected blocking size, as smaller areas exceed the threshold required for blocking to be identified. Further, decreased upper-level PV forces a weakening of blocking events together with a decrease in the detected duration. Thus, when comparing results from various models, it is important to consider any potential mean state differences in order to successfully attribute deviations in blocking frequencies to an actual difference in blocking activity rather than to mere mean state biases.

Finally, regarding the marked differences in blocking deviations when comparing the APV* with the AGP index, we conclude that the verification of atmospheric blocking in NWP models is highly sensitive to the blocking identification used, i.e. on the type of blocking the diagnostic is focusing on.

Acknowledgments

References

ALTENHOFF, A.M., O. MARTIUS, M. CROCI-MASPOLI, C. SCHWIERZ, H.C. DAVIES, 2008: Linkage of atmospheric blocks and synoptic-scale Rossby waves: a climatological analysis. – Tellus A **60**, 1053–1063, DOI: 10.1111/j.1600-0870.2008.00354.x.

ANSTEY, J.A., P. DAVINI, L.J. GRAY, T.J. WOOLLINGS, N. BUTCHART, C. CAGNAZZO, B. CHRISTIANSEN, S.C. HARDIMAN, S.M. OSPREY, S. YANG, 2013: Multi–model analysis of Northern Hemisphere winter blocking: Model biases and the role of resolution. – J. Geophys. Res. **118**, 3956–3971, DOI: 10.1002/jgrd.50231.

BARRIOPEDRO, D., R. GARCÍA-HERRERA, R.M. TRIGO, 2010: Application of blocking diagnosis methods to General Circulation Models. Part I: a novel detection scheme. – Clim. Dyn. **35**, 1373–1391, DOI: 10.1007/s00382-010-0767-5.

BERCKMANS, J., T. WOOLLINGS, M.E. DEMORY, P.L. VIDALE, M. ROBERTS, 2013: Atmospheric blocking in a high resolution climate model: influences of mean state, orography and eddy forcing. – Atmos. Sci. Lett. **14**, 34–40, DOI: 10.1002/asl2.412.

BIELI, M., S. PFAHL, H. WERNLI, 2015: A Lagrangian investigation of hot and cold temperature extremes in Europe. – Quart. J. Roy. Meteor. Soc. **141**, 98–108, DOI: 10.1002/qj.2339.

BLACK, E., M. BLACKBURN, G. HARRISON, B. HOSKINS, J. METHVEN, 2004: Factors contributing to the summer 2003 European heatwave. – Weather **59**, 217–223, DOI: 10.1256/wea.74.04.

BUEHLER, T., C.C. RAIBLE, T.F. STOCKER, 2011: The relationship of winter season North Atlantic blocking frequencies to extreme cold or dry spells in the ERA–40. – Tellus A **63**, DOI: 10.3402/tellusa.v63i2.15797.

CROCI-MASPOLI, M., H.C. DAVIES, 2009: Key dynamical features of the 2005/06 European winter. – Mon. Weather Rev. **137**, 664–678, DOI: 10.1175/2008MWR2533.1.

CROCI-MASPOLI, M., C. SCHWIERZ, H.C. DAVIES, 2007: A multifaceted climatology of atmospheric blocking and its recent linear trend. – J. Climate **20**, 633–649, DOI: 10.1175/JCLI4029.1.

D'ANDREA, F., S. TIBALDI, M. BLACKBURN, G. BOER, M. DÉQUÉ, M.R. DIX, B. DUGAS, L. FERRANTI, T. IWASAKI, A. KITOH, V. POPE, D. RANDALL, E. ROECKNER, D. STRAUSS, W. STERN, H.V.d. DOOL, D. WILLIAMSON, 1998: Northern Hemisphere atmospheric blocking as simulated by 15 atmospheric general circulation models in the period 1979-1988. – Climate Dyn. **14**, 385–407, DOI: 10.1007/s003820050230.

DAVINI, P., F. D'ANDREA, 2016: Northern Hemisphere atmospheric blocking representation in global climate models: Twenty years of improvements? – J. Clim. **29**, 8823–8840, DOI: 10.1175/JCLI-D-16-0242.1.

DAVINI, P., C. CAGNAZZO, S. GUALDI, A. NAVARRA, 2012: Bidimensional diagnostics, variability, and trends of Northern Hemisphere blocking. – J. Climate **25**, 6496–6509, DOI: 10.1175/JCLI-D-12-00032.1.

DAVINI, P., S. CORTI, F. D'ANDREA, G. RIVIÈRE, von J. HARDENBERG, 2017: Improved winter European atmospheric blocking frequencies in high-resolution global climate simulations. – J. Adv. Model Earth Syst. **9**, 2615–2634, DOI: 10.1002/2017MS001082.

DAVIS, S.M., M.I. HEGGLIN, M. FUJIWARA, R. DRAGANI, Y. HARADA, C. KOBAYASHI, C. LONG, G.L. MANNEY, E.R. NASH, G.L. POTTER, S. TEGTMEIER, T. WANG, K. WARGAN, J.S. WRIGHT, 2017: Assessment of upper tropospheric and stratospheric water vapor and ozone in reanalyses as part of S-RIP. – Atmos. Chem. Phys. **17**, 12743–12778, DOI: 10.5194/acp-17-12743-2017.

DAWSON, A., T.N. PALMER, 2014: Simulating weather regimes: impact of model resolution and stochastic parameterization. – Climate Dyn. **44**, 2177–2193, DOI: 10.1007/s00382-014-2238-x.

DEE, D.P., S.M. UPPALA, A.J. SIMMONS, P. BERRISFORD, P. POLI, S. KOBAYASHI, U. ANDRAE, M.A. BALMASEDA, G. BALSAMO, P. BAUER, P. BECHTOLD, A.C.M. BELJAARS, van de L. BERG, J. BIDLOT, N. BORMANN, C. DELSOL, R. DRAGANI, M. FUENTES, A.J. GEER, L. HAIMBERGER, S.B. HEALY, H. HERSBACH, E.V. HÓLM, L. ISAKSEN, P. KÅLLBERG, M. KÖHLER, M. MATRICARDI, A.P. MCNALLY, B.M. MONGE-SANZ, J.J. MORCRETTE, B.K. PARK, C. PEUBEY, P. DE ROSNAY, C. TAVOLATO, J.N. THÉPAUT, F. VITART, 2011: The ERA-Interim reanalysis: configuration and performance of the data

assimilation system. – Quart. J. Roy. Meteor. Soc. **137**, 553–597, DOI: 10.1002/qj.828.

DOBLAS-REYES, F.J., M. DÉQUÉ, F. VALERO, D.B. STEPHENSON, 1998: North Atlantic wintertime intraseasonal variability and its sensitivity to GCM horizontal resolution. – Tellus A **50**, 573–595, DOI: 10.1034/j.1600-0870.1998.t01-4-00002.x.

DOLE, R.M., N.D. GORDON, 1983: Persistent anomalies of the extratropical Northern Hemisphere wintertime circulation: Geographical distribution and regional persistence characteristics. – Mon. Wea. Rev. **111**, 1567–1586, DOI: 10.1175/1520-0493(1983)111<1567:PAOTEN>2.0.CO;2.

ELLIOTT, R.D., T.B. SMITH, 1949: A study of the effects of large blocking highs on the general circulation in the Northern–Hemisphere westerlies. – J. Meteorol. **6**, 68–85, DOI: 10.1175/1520-0469(1949)006<0068:ASOTEO>2.0.CO;2.

ERTEL, H., 1942: Ein neuer hydrodynamischer Wirbelsatz. – Meteorol. Z. **59**, 277–281.

FUJIWARA, M., J.S. WRIGHT, G.L. MANNEY, L.J. GRAY, J. ANSTEY, T. BIRNER, S. DAVIS, E.P. GERBER, V.L. HARVEY, M.I. HEGGLIN, C.R. HOMEYER, J.A. KNOX, K. KRÜGER, A. LAMBERT, C.S. LONG, P. MARTINEAU, A. MOLOD, B.M. MONGE-SANZ, M.L. SANTEE, S. TEGTMEIER, S. CHABRILLAT, D.G.H. TAN, D.R. JACKSON, R. POLAVARAPU, G.P. COMPO, R. DRAGANI, W. EBISUZAKI, Y. HARADA, C. KOBAYASHI, W. MCCARTY, K. ONOGI, S. PAWSON, A. SIMMONS, K. WARGAN, J.S. WHITAKER, C.Z. ZOU, 2017: Introduction to the SPARC Reanalysis Intercomparison Project (S-RIP) and overview of the reanalysis systems. – Atmos. Chem. Phys. **17**, 1417–1452, DOI: 10.5194/acp-17-1417-2017.

GATES, W.L., 1992: AMIP: The atmospheric model intercomparison project. – Bull. Amer. Meteor. Soc. **73**, 1962–1970, DOI: 10.1175/1520-0477(1992)073<1962:ATAMIP>2.0.CO;2.

GRAMS, C.M., H. BINDER, S. PFAHL, N. PIAGET, H. WERNLI, 2014: Atmospheric processes triggering the central European floods in June 2013. – Nat. Hazards Earth Syst. Sci. **14**, 1691–1702, DOI: 10.5194/nhess-14-1691-2014.

HOSKINS, B.J., M. MCINTYRE, A.W. ROBERTSON, 1985: On the use and significance of isentropic potential vorticity maps. – Quart. J. Roy. Meteor. Soc. **111**, 877–946, DOI: 10.1002/qj.49711147002.

LENGGENHAGER, S., M. CROCI-MASPOLI, S. BRÖNNIMANN, O. MARTIUS, 2018: On the dynamical coupling between atmospheric blocks and heavy precipitation events: A discussion of the southern Alpine flood in October 2000. – Quart. J. Roy. Meteor. Soc. **145**, 530–545. DOI: 10.1002/qj.3449.

MARTIUS, O., H. SODEMANN, H. JOOS, S. PFAHL, A. WINSCHALL, M. CROCI-MASPOLI, M. GRAF, E. MADONNA, B. MUELLER, S. SCHEMM, J. SEDLÁČEK, M. SPRENGER, H. WERNLI, 2013: The role of upper-level dynamics and surface processes for the Pakistan flood of July 2010. – Quart. J. Roy. Meteor. Soc. **139**, 1780–1797, DOI: 10.1002/qj.2082.

MASATO, G., B.J. HOSKINS, T. WOOLLINGS, 2013: Winter and summer Northern Hemisphere blocking in CMIP5 models. – J. Climate **26**, 7044–7059, DOI: 10.1175/JCLI-D-12-00466.1.

MATSUEDA, M., T.N. PALMER, 2018: Estimates of flow–dependent predictability of wintertime Euro-Atlantic weather regimes in medium–range forecasts. – Quart. J. Roy. Meteor. Soc. **0**, DOI: 10.1002/qj.3265.

MATSUEDA, M., R. MIZUTA, S. KUSUNOKI, 2009: Future change in wintertime atmospheric blocking simulated using a 20-km-mesh atmospheric global circulation model. – J. Geophys. Res. **114**, D12114, DOI: 10.1029/2009JD011919.

PASQUIER, J.T., S. PFAHL, C.M. GRAMS, 2019: Modulation of atmospheric river occurrence and associated precipitation extremes in the North Atlantic region by European weather

regimes. – Geophys. Res. Lett. **46**, 1014–1023, DOI: 10.1029/2018GL081194.

PELLY, J.L., B.J. HOSKINS, 2003: A new perspective on blocking. – J. Atmos. Sci. **60**, 743–755, DOI: 10.1175/1520-0469(2003)060<0743:ANPOB>2.0.CO;2.

PFAHL, S., H. WERNLI, 2012: Quantifying the relevance of atmospheric blocking for co–located temperature extremes in the Northern Hemisphere on (sub-)daily time scales. – Geophys. Res. Lett. **39**, L12807, DOI: 10.1029/2012GL052261.

PFAHL, S., C. SCHWIERZ, M. CROCI-MASPOLI, C.M. GRAMS, H. WERNLI, 2015: Importance of latent heat release in ascending air streams for atmospheric blocking. – Nature Geosci. **8**, 610–614, DOI: 10.1038/ngeo2487.

PIAGET, N., P. FROIDEVAUX, P. GIANNAKAKI, F. GIERTH, O. MARTIUS, M. RIEMER, G. WOLF, C.M. GRAMS, 2015: Dynamics of a local Alpine flooding event in October 2011: Moisture source and large-scale circulation. – Quart. J. Roy. Meteor. Soc. **141**, 1922–1937, DOI: 10.1002/qj.2496.

QUANDT, L.A., J.H. KELLER, O. MARTIUS, J.G. PINTO, S.C. JONES, 2019: Ensemble sensitivity analysis of the blocking system over Russia in summer 2010. – Mon. Wea. Rev. **147**, 657–675, DOI: 10.1175/MWR-D-18-0252.1.

REX, D.F., 1950: Blocking action in the middle troposphere and its effect upon regional climate. – Tellus A **2**, DOI: 10.3402/tellusa.v2i4.8603.

SCAIFE, A.A., T. WOOLLINGS, J. KNIGHT, G. MARTIN, T. HINTON, 2010: Atmospheric blocking and mean biases in climate models. – J. Clim. **23**, 6143–6152, DOI: 10.1175/2010JCLI3728.1.

SCHERRER, S.C., M. CROCI-MASPOLI, C. SCHWIERZ, C. APPENZELLER, 2006: Two-dimensional indices of atmospheric blocking and their statistical relationship with winter climate patterns in the Euro-Atlantic region. – Int. J. Climatol. **26**, 233–249, DOI: 10.1002/joc.1250.

SCHIEMANN, R., M.E. DEMORY, L.C. SHAFFREY, J. STRACHAN, P.L. VIDALE, M.S. MIZIELINSKI, M.J. ROBERTS, M. MATSUEDA, M.F. WEHNER, T. JUNG, 2017: The resolution sensitivity of Northern Hemisphere blocking in four 25-km atmospheric global circulation models. – J. Climate **30**, 337–358, DOI: 10.1175/JCLI-D-16-0100.1.

SCHWIERZ, C., M. CROCI-MASPOLI, H.C. DAVIES, 2004: Perspicacious indicators of atmospheric blocking. – Geophys. Res. Lett. **31**, L06125, DOI: 10.1029/2003GL019341.

SMALL, D., E. ATALLAH, J.R. GYAKUM, 2013: An objectively determined blocking index and its Northern Hemisphere climatology. – J. Climate **27**, 2948–2970, DOI: 10.1175/JCLI-D-13-00374.1.

STENKE, A., V. GREWE, M. PONATER, 2008: Lagrangian transport of water vapor and cloud water in the ECHAM4 GCM and its impact on the cold bias. – Climate Dyn. **31**, 491–506, DOI: 10.1007/s00382-007-0347-5.

SUMNER, E., 1954: A study of blocking in the Atlantic – European of the Northern Hemisphere. – Quart. J. Roy. Meteor. Soc. **80**, 402–416, DOI: 10.1002/qj.49708034510.

TIBALDI, S., F. MOLTENI, 1990: On the operational predictability of blocking. – Tellus A **42**, 343–365, DOI: 10.1034/j.1600-0870.1990.t01-2-00003.x.

VIAL, J., T.J. OSBORN, 2011: Assessment of atmosphere-ocean general circulation model simulations of winter Northern Hemisphere atmospheric blocking. – Climate Dyn. **39**, 95–112, DOI: 10.1007/s00382-011-1177-z.

WATERS, J.W., L. FROIDEVAUX, R.S. HARWOOD, R.F. JARNOT, H.M. PICKETT, W.G. READ, P.H. SIEGEL, R.E. COFIELD, M.J. FILIPIAK, D.A. FLOWER, J.R. HOLDEN, G.K. LAU, N.J. LIVESEY, G.L. MANNEY, H.C. PUMPHREY, M.L. SANTEE, D.L. WU, D.T. CUDDY, R.R. LAY, M.S. LOO, V.S. PERUN, M.J. SCHWARTZ, P.C. STEK, R.P. THURSTANS, M.A. BOYLES,

K.M. Chandra, M.C. Chavez, G.S. Chen, B.V. Chudasama, R. Dodge, R.A. Fuller, M.A. Girard, J.H. Jiang, Y. Jiang, B.W. Knosp, R.C. LaBelle, J.C. Lam, K.A. Lee, D. Miller, J.E. Oswald, N.C. Patel, D.M. Pukala, O. Quintero, D.M. Scaff, W.V. Snyder, M.C. Tope, P.A. Wagner, M.J. Walch, 2006: The Earth observing system microwave limb sounder (EOS MLS) on the aura Satellite. – IEEE Trans. Geosci. Remote Sens. **44**, 1075–1092, DOI: 10.1109/TGRS.2006.873771.

Zängl, G., D. Reinert, P. Rípodas, M. Baldauf, 2015: The ICON (ICOsahedral Non-hydrostatic) modelling framework of DWD and MPI-M: Description of the non-hydrostatic dynamical core. – Quart. J. Roy. Meteor. Soc. **141**, 563–579, DOI: 10.1002/qj.2378.